Prediction of nanographene binding-scores to trout cellular receptors and cytochromes

Connolly, M., C., Navas, J.M. and Coll, J*.
Department of Environment. Instituto Nacional de Investigacion y Tecnología Agraria y Alimentaria, INIA. Madrid, Spain.
short title: nanographenes AHR and CYP bindings
Keywords: nanographene fragment; AHR; CYP; P450; trout; virtual binding; docking; ligands;

Connolly, Mona email: connolly.mona@inia.es orcid: 0000-0003-3574-8564
Navas, Jose María email: jmnavas@inia.es orcid: 0000-0002-7644-8499
* Corresponding author Coll, Julio email: juliocollm@gmail.com orcid: 0000-0001-8496-3493

Abstract: To address the increasing concerns surrounding possible impacts of graphene-related materials on the aquatic environment, this study focused on computational predictions of binding between models of graphenes in the nm size range (nanographenes, nGs) and the aryl-hydrocarbon receptor (tAHR) and P450 cytochromes (tCYPs) of rainbow trout (*Oncorhynchus mykiss*). The tAHR plays a key role in the induction of detoxifying and early immune responses and tCYPs are essential for detoxifying planar hydrophobic chemicals such as nGs. After 3D modelling of those trout proteins, docking algorithms predicted the size-dependance profiles of nGs binding-scores to tAHR and tCYPs in the low nM range (high binding-affinities). Virtual oxidations of nGs to nGOs (carboxy-, epoxy- and/or hydroxy-oxidations) further lowered the corresponding binding-scores in level/type-oxidation manners. Among all the tCYPs, the tCYP3AR (the equivalent to human CYP3A4) was identified as a potential key interaction enzyme for nGs because of its lower binding-scores. These results implicate a possible processing pathway to be further probed through *in vitro* and *in vivo* experimentation. Together the information generated can be pivotal for the design of safer graphene-related materials for a variety of applications and help to understand their detoxification in aquatic vertebrates.

Introduction

Graphene-related materials (GRMs) have potential applications in a variety of human activities, from aeronautics to biomedicine, to electronics and in agriculture. This is causing a constant increase in the production of GRMs that will likely lead to releases to the environment during production, use and/or disposal [1]. Although the current concentrations and toxicological hazards of GRM in the aquatic media are yet minimal, they are expected to increase with graphene production [2-4]. Usually, graphene is not used in its pristine form but with a certain degree of oxidations (GOs). GOs have been shown to interact with other environmental pollutants, such as polyaromatic hydrocarbons (PAHs) causing an increase in cytotoxicity as estimated in fish cell lines [5]. Once in the aquatic environment, residues of GOs will likely interact with a variety of biota but there is only a limited knowledge of the bio-reactions they might induce. Among these bio-reactions, perturbations in detoxifying mechanisms [6] and immune responses [7-9] would have important impacts on vertebrates. To better understand the possible initiation of detoxyfying bio-reactions induced by or interfering with GOs, we have selected small fragments or nanographenes (nGs) to mimic degradation products of larger sheets. In this study we have focused on the possible effects of pristine nanographenes considering those as a single layer sheet < 100 nm lateral size without (nGs) and with different levels of oxidation (nGOs).

Previous work has shown that nGOs can adhere to the cellular plasma membrane, insert into the lipid bilayers and enter the cytoplasm [10]. Once inside the cell, detoxification pathways could be activated that may hypothetically include receptor binding and induction of enzymes that cause a reduction of hydrophobicity by further oxidation (including carboxy- epoxy- and hydroxy-oxidation) to more hydrophilic metabolites which could more easily be excreted via the bile, urine or gills to prevent toxic concentrations and their derived bio-effects [11, 12]. We hypothesize that extracellularly, large graphenes (platelets) may begin their degradation by different mechanisms such as oxidation with reactive oxygen produced by peroxidases [13, 14], leading to nGO. Alternatively, and although not yet demonstrated, different intramolecular imperfections in the graphene platelets could allow oxidations to occur extracellularly. Once inside cells, nGOs could bind to the aryl-hydrocarbon receptor (AHR) and induce oxidating cytochromes (CYPs), that will feed-back to further accelerate oxidation.

Taking into account the hypothesis mentioned above, we have computationally explored whether nGs/nGOs of ~25-200 rings could bind to intracellular AHR and/or CYPs with enough binding affinity to explain any downstream effects. Given the large differences among nGOs derivatives, it would be most convenient to select only those with the highest likelihood to elicit such bio-reactions that could be then demonstrated through *in vitro* or *in vivo* experimentation. Any reduction in the number of possibilities would make experimentation approaches more targeted and feasible. Therefore, to improve the likelihood of experimental success and to increase our understanding of possible detoxification mechanisms, *in silico* binding predictions between nGs/nGOs and 3D modeled AHR / CYPs has been performed.

For this work, rainbow trout (*Oncorhynchus mykiss*) was selected as a model vertebrate species because of their high sensitivity to environmental pollutants, and widespread use in ecotoxicological studies. Additionally, a number of their detoxifying and immune-related genes and/or functionalities have been studied. Therefore, this work specifically focuses on the trout aryl-hydrocarbon receptor (tAHR) and detoxification cytochrome enzymes such as CYPs (tCYPs).

Single layer graphene is constituted by a series of aromatic rings forming a planar structure. Therefore, Gs/GOs are structurally related to PAHs which are also constituted by aromatic rings albeit PAHs have a much lower number of rings. Since the AHR is one of the first proteins to recognise the intracellular presence of PAHs, we have hypothesized that the AHR could also bind nGs/nGOs. Once bound to a ligand, the cytoplasmic AHR dissociates from HSP90 and other proteins, binds to the aryl-hydrocarbon receptor nuclear translocator protein (ARNT) [15] and translocates into the cell's nucleus. The co-transcriptional factor AHR/ARNT complex then interacts with xenobiotic genomic DNA response elements (XREs) to induce transcription of *cyps* and many other proteins [16]. The recognition of ligands by PAHs has been mapped in mammalian AHRs to their PAS domain (PER, ARNT, SIM) which is common to other proteins of the same family of transcriptional factors. In particular, deletion analysis demonstrated that the binding-domain was localized in the amino-terminal part of AHR at residues 1-403. In contrast, deletion of 398-805 residues had no effect on ligand binding [17, 18]. Mouse AHR mutants at the 375 residue confirmed a reduction of binding of the prototypical ligands [19]. Although all the above mentioned properties are most probably similar in trout, confirmatory studies are very scarce and some AHR downstream pathways may differ [20].

Detoxification of target aromatic molecules like PAHs, begins with the so called detoxification phase 1 by the addition of -COOH, -O, or -OH, by monooxygenases (predominant), flavoprotein monoxygenases, monoamine oxidases, epoxide hydrolases and/or reductases. Among all these possibilities, CYPs were chosen for this study because in vertebrates these oxidative microsomal-membrane heme-containing enzymes are the main participants in phase 1 detoxyfication [21]. In addition, some of them are induced after ligand binding to AHR and have been studied in rainbow trout [22], to such an extent that induction of CYP1 by AHR activation is been used as a biomarker for hydrophobic contaminant exposure [23, 24]. A feed-back loop regulates AHR and CYPs transcription, increasing CYP1 down-regulates *ahr* and inhibition of CYP1 up-regulates *ahr* [16]. In human cells, inhibition of CYP1 up-regulates also helper T cells (and other immune cells) while down-regulating *il17* gene expression [25]. Furthermore, some of the CYPs effects during infections resemble those of proinflammatory cytokines, further implicating CYPs in inflammation and immunology [26].

Putative CYPs predicted in their corresponding genomes (http://drnelson.uthsc.edu/cytochromeP450.html), showed species- and family-specific amino acid sequences [22], nevertheless with high tridimensional 3D structural similarities. CYPs are divided into those involved in xenobiotic catabolism (CYP1-4) and those implicated in metabolic biosynthesis (CYP5-51). Some CYPs are constitutively expressed but others are induced by PAHs [27]. Specifically in fish, many CYP enzymes are known to be implicated in fish metabolic biosynthesis such as that of hydroxycholesterols [28], but also several CYP1-4 detoxyfying enzyme families have been detected [22]. Therefore, it is expected that most foreign compounds introduced into the cellular environment of a fish body, including nGs/nGOs, could hypothetically interact with several CYPs as well as with other detoxifying enzymes. Furthermore, structurally distinct nGs/nGOs may have specific binding affinities with different CYPs with either inhibitory or synergistic results.

Therefore, this work focuses on prediction of binding-scores and conformations or binding-poses of pristine nGs and oxidated nGOs with tAHR and tCYPs. To our knowledge, no such computational predictions have been yet reported for any graphene-like or nGs/nGOs to tAHR/tCYPs [6, 29-31].

Materials and Methods

Nanographene ligands

Graphene-like ligands were obtained by a similarity search in PubMed (https://pubchem.ncbi.nlm.nih.gov/#query=C1%5BC%40%40H%5D2N%3DN%5BC%40%40H%5D3%5BC%40H%5D1C1%3DC(C%3DCC%3DC1)%5BC%40H%5D23&tab=similarity) by providing an 8 ring graphene-like molecule (SMILES= C1=CC2=C3C=CC4=CC=C5C=CC=C6C7=CC=C8C=CC(=C1)C2=C8C7=C3C4=C56) corresponding to Zinc ID 104923703 (http://zinc15.docking.org/). The corresponding downloaded sdf file manually curated, contained 86 small molecular weight graphene-like compounds.

To mimic graphene platelet degradation products, pdb models of nanographene (called nGs here, because of their 10-200 nm lateral side range) were designed and obtained using the open-source Phyton GOPY tool (https://github.com/lourarum/GOPY). The nGs were obtained in different sizes (4 to 156 rings), and with different levels of oxidation (carboxylation -COOH, epoxy oxidation -O- , hydroxylation –OH and/or combinations). Oxygens were added to a maximum of ~1.6 Carbon/Oxygen C/O ratio, similar to those described in previous experimental work [32]. While carboxylation can occur only at the C edges, both epoxyoxidation and hydroxilation may occur at each of the Cs inside the rings to be distributed randomly between the two faces of the planar nG sheet (see some depictions in Figure S3). In all cases, steric hindrance may reduce the number of theoretical possibilities. Ten random designs for each of the oxidation scenarios were computationally constructed for each oxidation state by modifications of the Phyton GOPY tool, which took into account all the requirements mentioned above [33]. The resulting nanographene structures visualized in PyMOL showed a variety of numbers and intramolecular locations approximating the input numbers provided to the GOPY tool because of steric restrictions. Additionally, docking analysis rejected 10-20% of the structures specifically when 2 oxidations were too close in the same ring.

Tridimensional trout AHR and CYP 3D models

The trout AHR (tAHR) was modeled using the SWISS- MODEL homology modeling (https://swissmodel.expasy.org/interactive). Structural similarities were expressed in Angstroms Å / number of common atoms, as estimated by 3D superposition with hAHR-1 in the CCP4 Molecular Graphics program vs2.10.11 (http://www.ccp4.ac.uk/MG) (Table 1)

The trout CYP (tCYP) enzymes selected for this work corresponded to those sequence-reviewed, that were available for *Oncorynchus mykiss* and downloaded from UNIPROT (https://www.uniprot.org/uniprot/?query=reviewed:yes). They corresponded to most of the best studied tCYPs [22]. Human eosinophil peroxidase or myeloperoxidase, was also included for comparison with previous work because to our knowledge it was the only CYP enzyme used in a previous nG oxidation computational study [34]. The amino acid sequences were submitted to the SWISS- MODEL to obtain hypothetical 3D models. The coordinates of the heme and ligand binding pockets provided by the CYP human templates were copied from the human pdb to the modeled trout pdb file (Research Collaboratory for Structural Bioinformatics, RCSB, Protein Data Bank PDB). All modeled structures were visualized in PyMOL and PyRx . Structural similarities were studied as commented above by 3D superposition with tCYP1A1.Predicted binding pockets and α-helices were investigated using the seeSAR vs.10 program (https://www.biosolveit.de/SeeSAR/).

AutoDock Vina virtual docking

The AutoDock Vina program [35] included in the PyRx 0.9.8. package [36] (https://pyrx.sourceforge.io/) was used in e7 desk computers to predict Gibbs free-energy (ΔG) as described before [28, 37, 38], using grids including the whole protein molecules (blind docking) or the identified binding pockets when defined in the CYP templates. The *.sdf files were converted to *.pdbqt files by allowing ligand rotatable bonds, adding protonation and adding Gasteiger−Marsili partial atomic charges with one ffu energy minimization step carried out by the Open Babel program included into the PyRx package. Water molecules were not considered. Only the binding-poses with the lowest binding energy of each *.out.pdbqt were retained for further analysis. The output ΔG energies were converted to constant inhibition (Ki) values in molar concentrations (M), using the formula Ki = exp([ΔG × 1000] / [R × T]) (R = 1.98 cal/mol, and T = 298 °C)[39]. Final values were converted to nM. The predicted structures were visualized in PyRx and/or PyMOL (https://www.pymol.org/).

SeeSAR modeling

The seeSAR seeSAR vs.10 package (https://www.biosolveit.de/SeeSAR/) [40-42] was used for binding pocket predictions and alternative visualization of bound complexes as described previously[28, 37, 38]

Results

3D Modeling of trout AHR

One of the requirements for this study was to obtain a 3D model of the PAS domain of trout AHR (tAHR) based on the two amino acid sequences of tAHR available (97% identical) and some corresponding 3D solved structures. Since only residues 107-261 of human AHR (hAHR) were crystallographically solved and those were not enough to cover all the corresponding hAHR ligand binding domains, a template search was undertaken for a better template. Seven hAHR models were selected by the SWISS-model program using template PAS domains from diverse proteins including those from similar transcription factors. Among them, 6 models showed < 2 Å RMSD differences in their 3D structure alpha-carbons. The hAHR-1 model covering the highest number of amino acids of 357 residues was selected (Table 1, highlighted in grey background) to model the two tAHRs. The resulting modeled tAHRa and b structures were very similar (Table 1, last entries).

Table 1. Modelling of human and trout AHR

name	protein sequence	#aa	SWISS template	#aa 3D modeled	SI, %	RMSD, Å/#atoms
hAHR	NM_001621	848	4m4x	107-261	100	1.92/103
hAHR-1	NM_001621	848	5sys5	34-391	28.7	0.00/360
hAHR-2	NM_001621	848	4f3l	35-391	24.7	1.27/99
hAHR-3	NM_001621	848	4f3l	29-381	24.8	2.74/122
hAHR-4	NM_001621	848	5sy5	36-381	21.2	1.88/115
hAHR-5	NM_001621	848	4zpk	32-386	29.5	1.99/258
hAHR-6	NM_001621	848	4f3l	36-381	26.6	1.17/95
hAHR-7	NM_001621	848	5sy7	33-373	26.4	5.48/104
tAHRa	AF065137	1058	hAHR-1	34-391	71.2	0.38/348
tAHRb	AF065138	1059	hAHR-1	34-391	71.2	0.38/348

The sequences were obtained from the NUCCORE databank. Protein sequences from PAS domain of the hHRA (residues 1 to 420) were submitted to the SWISS-MODEL homology modelling, which automatically selected 7 possible templates with the highest sequence identity (SI). The hHRA-1 (highlighted grey background) was selected as model template for tAHRa and b. tHRAa and b sequences showed 97 % SI. hAHR, human AHR.
#aa, number of amino acids.
RMSD, Structural similarity in Å / number of common atoms by 3D superposing to hAHR-1 in CCP4.

Table 2. Modelling of trout CYPs compared to human myeloperoxidase hEPO

name	protein sequence	#aa	SWISS template	human template	SI, %	RMSD, Å/#atoms
tCYP1A1	Q92110	522	4i8v	CYP1A1	58.9	0.00/522
tCYP1A3	Q92109	522	4i8v	CYP1A1	59.3	0.04/469
tCYP2K1	Q92090	504	2pg6	CYP2A6	41.1	1.85/423
tCYP2K3	093299	490	1nr6	CYP2D5	41.4	1.89/395
tCYP2K4	O93297	504	2pg6	CYP2A6	40.7	1.86/426
tCYP2M1	Q92088	499	1suo	CYP2B4	47.8	1.80/397
tCYP3AR	O42563	518	1tqn	CYP3A4	55.9	2.29/377
tCYP11A	Q07217	514	3n9y	CYP11A1	50.8	2.76/377
tCYP17A	P30437	514	6b82	CYP17A1	75.7	1.86/418
hEPO	P05164	745	-------	1mhl	-----	--------

Only trout CYP protein sequences reviewed in UNIPROT were downloaded and modeled. Protein sequences were modeled as in Table 1. The coordinates of the heme and ligand binding pockets were copied from the human pdb to the modeled trout pdb file and visualized in PyMOL.
hEPO, human eosinophyl peroxidase or myeloperoxidase enzyme-degrading graphene, included for comparison with previous work [34].
#aa, number of amino acids.
RMSD, Structural similarity.

3D Modeling of trout CYPs

Because of the absence of crystallization studies that solved the structures of trout CYPs (tCYPs), their hypothetical 3D structures were modeled for the first time (Table 2, Figure S1). Despite the differences in their amino acid sequences (Table S1), all the tCYP models have similar overall 3D structures as shown by their < 3 Å RMSD. The tCYP 3D structures have several α-helices, one conserved Cysteine, and an inner heme. Their carboxy-terminal helices contain a highly conserved domain (Table S1, red amino acids). Heme binding implicating residues ~100-140 and ~300-320 were in the pM range, as shown by seeSAR. An amino-terminal tunnel-like access (Figure S1, grey arrow) may be the main route for substrates/inhibitors to penetrate nearby the heme for optimal oxidation. A binding pocket predicted by seeSAR, was identified around the heme in all tCYPs (Figure S1, yellow pocket).

Computational binding of nG-like compounds to hAHR and tAHR

Most but not all nG-like compounds showed similar binding-scores to h and tAHR despite their differences in amino acid sequences (Figure 1A). Nevertheless, their corresponding nG binding-poses were different (Figure 1B and C).

Among the nG-like compounds there was a reduction of binding-scores down to 10^{-4} nM with increasing number of rings per molecule, in the following order, circumanthracene (13 rings), circumcoronene (19), circumvalene (24), nG (25) and circumcircumcoronene (37).

Since there were no differences between the binding-scores of tAHRa and b (not shown), the tAHRa model was selected for the rest of the work. Our approach predicted binding-scores in the 10^3 nM range for the hAHR prototypical agonist 2,3,7,8-tetrachlorodibenzo-para-dioxin (TCDD) (not shown).

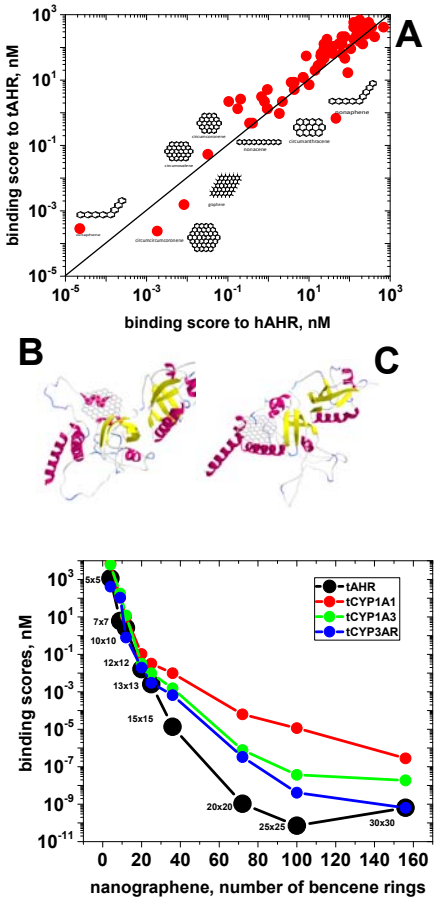

Figure 1. Binding-scores of nG-like compounds to hAHR and tAHR.
A) Binding-scores to 83 nG-like compounds compared between hAHR and tAHR.
B) Drawing showing the best pose of 37-ring nG bound to hAHR.
C) Drawing showing the best pose of 37-ring nG bound to tAHR.

Figure 2. Influence of the number of rings of nG in their binding to tAHR and to tCYPs.
nGs of different sizes were designed by the GOPY tool.
Black numbers, lateral sizes in nm of the nGs for inputs to the GOPY tool.
Black circles, tAHR.
Red circles, tCYP1A1.
Green circles, tCYP1A3.
Blue circles, tCYP3AR.

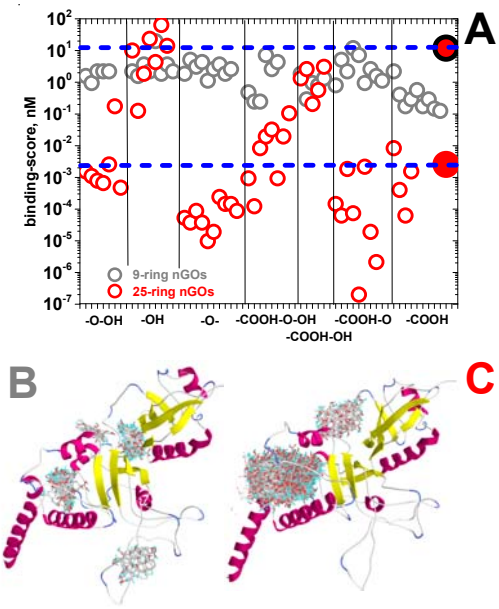

Figure 3. Influence of nG oxidation(nGO) in the binding-scores to tAHR. Oxidations with –COOH, -O- , -OH and combinations of them were randomly added at maximal C/O ~1.6 ratios to 9 or 25-ring nG using the GOPY tool.
A) Grey-edged circles, 9-ring nGO.
Red-edged circles, 25-ring nGO.
Grey-edge, red filled circle, 9-ring nG.
Red-edge red filled circle, 25-ring nG.
Black vertical lines, separation between different types of oxidations.
Dashed horizontal blue lines, nGs binding-scores to tAHR.
B) Mapping of 9-ring nGOs bindings to tAHR.
C) Mapping of 25-ring nGOs bindings o tAHR.

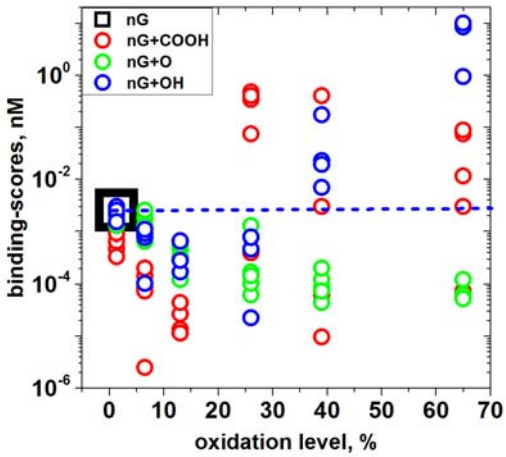

Figure 4. Influence of the level of oxidation in the binding of nGs to tAHR. Individual –COOH, -O- , -OH oxidant molecules were randomly added into 25 rings (77 Carbons) nGs by the GOPY tool. From 5-10 nG molecules were virtually oxidated per each level of oxidation. Due to steric problems when > 20-30 atoms were added, some of the resulting nGO structures when examined in PyMOL, only approximately confirmed the initial numbers supplied to the tool. Theoretical oxidations per nG molecule were expressed in % as calculated by the formula, 100 x number of output oxidative molecules per 77 Carbons.
Black big square and blue-dashed horizontal line, binding-scores of 5x5 nm nGs (mean of n=5).
red circles, nG+COOH.
Green circles, nG+O.
Blue circles, nG+OH.

Modeling of 20x20 nm nGs resulted in nGs of 72 rings down to binding-scores of >10^{-10} nM, compared to those of 25 nG or 37 circumcircumcoronene rings which bound to the hAHR / tAHR with binding-scores in the ~ 10^{-3} nM range (Figure 1A). To further investigate the influence of nG size in the binding to tAHR and tCYPs, different sizes were designed and computationally tested by blind docking (PAS tAHR domain) or binding-pocket docking (tCYPs).

The results predicted that the lower binding-scores to tAHR corresponded to nGs > 100-rings. Larger nGs maintained these binding-scores. Binding to tCYPs showed a similar size-profiles as to tAHR, but in the 10^{-5}-10^{-9} binding-score ranges (Figure 2, blue, green and red lines). Most tAHR binding to nGs mapped to its PAS ligand binding site. In contrast, most nGs binding to CYPs were localized on their surfaces away from their heme sites, suggesting some unspecific bindings (Figure S2). Only 4-9-ring nGs were mapped nearby to their heme site, most probably because only such small compounds could penetrate through the CYP tunnels to such internal location to be specifically oxidized (Figure S2).

Models of 9 (7x7 nm, 32 Carbons) and 25 (13x13 nm, 77 Carbons)-ring nGs were selected for further studies, because significant binding-scores could be obtained in minimal computational times.

Computational binding of nGOs to tAHR

Carboxy (-COOH), epoxy (-O-) and hydroxy (–HO) oxidations were mimicked by adding them to the 9 and 25-ring nGs to randomly generate their corresponding nGOs using 1.6 Carbon/Oxygen C/O ratios [10] (see some of their structures in Figure S3).

In this test, docking conditions were adjusted to yield binding-scores of ~10^{-3} nM and ~10^{1} nM for 25- and 9-rings nGs, respectively. Results with nGOs predicted 10^{1}-10^{-7} nM binding-scores for 25-rings (Figure 3,) and 10^{0} nM for most 9-rings (Figure 3, red- and grey-edged circles, respectively). In particular, epoxidation (-O-) alone or in combination with carboxylation (-COOH), was the most efficient process to reduce the binding-scores of 25-ring nGOs. In contrast, hydroxylation (-OH), and its combinations increased their binding-scores.

Mapping of the corresponding 3D binding-poses predicted that the amino terminal end of the PAS domain of tAHR was targeted by most 25- and 9-rings nGOs (Figure 3C and B, respectively).

Computational binding of nGOs with different oxidation levels

To study the influence of the levels of nGO oxidation on the binding to tAHR, different numbers of oxygen-containing molecules were added to 25-ring nGs. Results showed that increasing the level of peroxidation (-O-) to 70 % caused a continuous reduction to 10^{-4} nM binding-scores (Figure 4, green circles). Increasing the level of carboxylation (-COOH) or hydroxilation (-OH) to <25 % reduced their binding-scores to ~10^{-5}-10^{-6} nM , but increased them at higher oxidation levels (Figure 4, red and blue circles). Both nG and most nGO binding-scores to tAHR remained < 10^{1} nM, which may be significant compared to the 10^{3} nM binding-score of the AHR prototypical agonist TCDD under the same docking conditions.

Because of the nGs tendency to bind non- specifically to tCYPs (Figure S2), the size of the nGs were reduced to 5x5 nm (4 rings) and grids of 25 x 30 x25 Å surrounding the tCYPs heme were used for docking.

Under the above mentioned conditions, the nG binding-scores varied for each tCYPs molecular species from 10^2 to 10^4 nM (Figure 5, black-dashed horizontal lines). By increasing the level of nGOs oxidation to ~ 25 % most binding-scores decreased to different minimal levels for different tCYPs. However, increasing the level of most oxidations > 25 %, resulted in increased binding-scores for most tCYPs, except tCYP3AR. Thus, with >25 % oxidations, tCYP3AR binding-scores were further reduced to 10^{-2} by carboxylation (Figure 5, 3AR, red circles), and to a lower extent by peroxidation and hydroxylation.

Discussion

Lateral sizes of commercial powered graphene are of ~10 nm while the so called nanoplatelets range between 20-100 nm for oxidized graphene (GO) and between 100-1000 nm for carboxylated graphene [10]. Our initial working hypothesis was that larger graphene fragments (e.g., platelets) are broken down and taken up by trout cells transformed into smaller graphene pieces of ~10-100 rings (graphenes in the nm size range, here called nGs). We hypothesized that once internalized by cells, nGs/nGOs may interact with microsomal tAHR activating phase I detoxification mechanisms, such as those implicating peroxidase-dependent reactive oxygen [13, 14] and/or tCYPs enzymatic activities/*tcyp* gene transcription, to induce other bioeffects. All these possibilities remain largely unexplored.

To test such hypothesis by *in vitro* and *in vivo* experimentation, given the large numbers of different nGs/nGO derivatives, their numbers need to be reduced and possible candidates identified for further experimental studies. To do that, we proposed an *in silico* screening to select for those nGs with the highest binding affinities (lower binding-scores) to tAHR and tCYPs. We discovered that the maximal number of nG rings that tAHRs/tCYPs could bind is up to 25-rings with apparent binding-scores between 10^3-10^{-11} nM and mapping to the PAS tAHR specific binding site defined by its prototypical TCDD ligand.

Increasing hydrophilicity that facilitates detoxification of graphenes, is mostly caused by carboxylation, peroxidation and/or hydroxylation, but ring-opening and reduction may also be implicated [43].Oxidation of nGs to nGOs by virtually adding -COOH, -O- and –OH such as those expected to be found in most graphenes used for biomedical applications, computationally predicted between 10-100-fold reduction in their nG binding-scores to tAHR depending on the numbers of oxidated carbons per molecule and the type of oxidation. Additionally, any possible implication of tCYPs in nG binding and subsequent oxidation may be sterically possible only with the smallest nGs according to the computational data. Predicted conformation or pose analysis showed that although nGs could bind tCYPs, most of those bindings seem to be unspecific or not specifically oxidative because of their excessive separation from the inner tCYP heme where oxidation is expected to be most active. Pose bindings nearby the tCYP heme could not be visualized for nGs > 4 rings. Only the minimal nGs of 4 rings were small enough to penetrate the inner heme located within the predicted binding pockets.

With such size restrictions, among all the CYPs, the tCYP3AR was predicted to bind stronger than other tCYPs to nGOs, specifically to those which were carboxylated at their edges. Perhaps the higher implication of tCYP3AR in additional oxidations compared to other tCYPs may be due to its participation in the metabolism of endogenous substrates, such as steroids [43]. According to the UNIPROT data base, tCYP3AR is coded by the trout gene *cyp3a27*, however 3D modeling choose the human hCRP3A4 as the closest isomer, suggesting that despite nucleotide sequence differences, tCYP3AR is equivalent to hCYP3A4. Although our knowledge of any tCYPs is still scarce, immunologically relatedness of fish CYP3A to hCYT3A4 and rat CYP3A has been demonstrated [44]. However, since there is evidence that tCYP3A4 shows no significant bio-effects to seven known substrates of the corresponding hCYP3A4 [45], the impact of substrate oxidation may differ among species. The hCYP3A subfamily is the most important of drug-metabolizing enzymes since it accounts for ~30 % of the total CYPs in the liver and metabolizes ~50 % of marketed drugs [43]. In humans it is being expressed mainly in the liver where it accounts for 13 % of the total CYP content and has been implicated in the metabolism of ~4% of marketed drugs [43]. In contrast, few data are available for tCYP3AR.

The computational predictions identified the nGs molecular characteristics required to be suitable ligands for tAHR and therefore those with the higher potential to generate bio-effects. It may be hypothesized that subsequent translocation into the nucleus to induce the numerous tAHR-dependent genes would sustain the bases for a link between the environment and toxicological and immune responses at the cellular level. Although there are still no experimental evidences for that possibility, the present results indicate this may deserve futher explorations.

On the other hand, since vertebrate AHRs are expressed in many cells of both innate and adaptive immunity, the AHR may be one of the translators of environmental hydrophobic contamination into immunological responses. Experimental validation of such hypothesis, could be performed by *in vitro* and/or *vivo* assays by measuring the effect of synthetic nGs and their nGOs oxidated derivatives with different levels of oxidation, similar to those which have been investigated here using *in silico* screening.

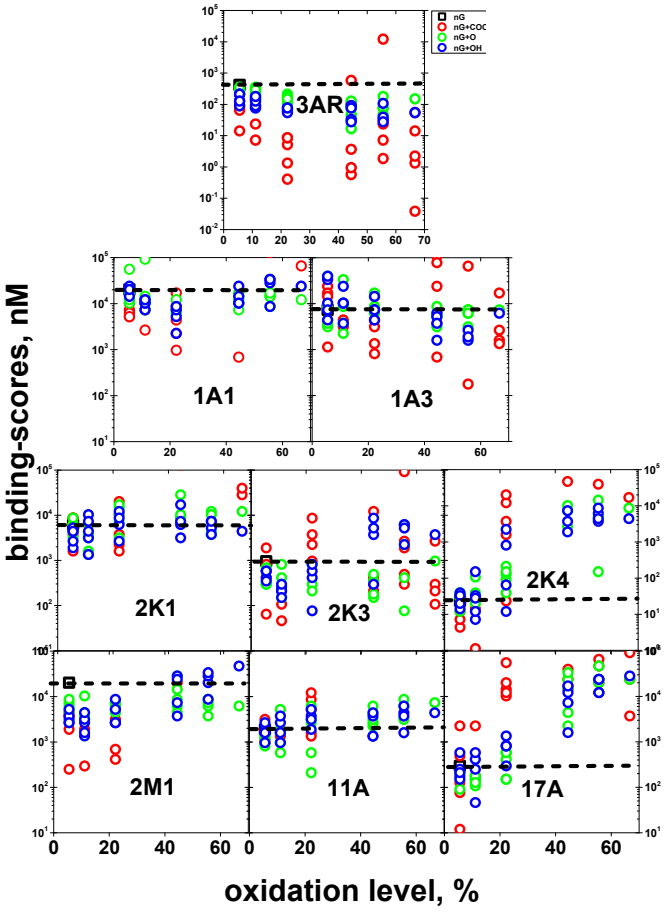

Figure 5. Influence of the level of oxidation in the binding of nGOs to tCYPs. Individual –COOH, -O- , -OH oxidant molecules were virtually and randomly added into 4 rings, 18 Cs nGs by the GOPY tool. From 5-10 nG molecules were virtually oxidated per each level of oxidation. Due to steric problems when > 20-30 atoms were added, some of the resulting structures examined in PyMOL only approximately confirmed the initial numbers supplied to the tool. Theoretical oxidations per nG molecule were expressed in % as calculated by the formula, 100 x number of oxidation molecules provided to the GOPY tool / 18 (n=5). The CYP family is in black bold lettering placed at around the 10^2 nM label for easy reference. Only those nGs showing binding affinities <10^5 nM were shown. All the scales were equal except the wider lower scale down to 10^{-2} for tCYP3AR.
Black big square and dashed horizontal line, binding-scores of 5x5 nm nGs (mean of n=5).
red circles, nGO-COOH.
Green circles, nGO-O-.
Blue circles, nG-OH.

Among the main difficulties to experimentally validate any hypothesis related to nG/nGO is the lack of such molecularly defined graphenes. An alternative to obtain the corresponding nGs/nGOs for experimental purposes could include not only chemical synthesis (if chemical synthesis could make it possible) but also strong sonication techniques or long peroxidation of graphene platelets. Techniques for removal of the largest fragments by ultracentrifugation and/or gel filtration chromatography are available. However, more detailed molecular characterization of such preparations than those routinely employed may also be required.

For further downstream experimentation, several *in vitro* assays such as those using subcellular fractions, fish cell lines, hepatocytes and/or tissues [24], could be used. Specifically to detect a variety of tAHR induced genes, for instance, RTqPCR could be used to detect up-/down-regulation of selected *tcyps.* Any induced tCYP1A and/or tCYP3A enzyme activities can also be monitored using ethoxyresorufin-O-deethylas(EROD) or benzyloxy-4-trifluoromethylcoumarin-O-debenzyloxylase (BFCOD) activity assays, respectively. To estimate possible induced immunological responses and/or to explain differences among AHR modulations observed across species[46], concentration-dependent effects on trout immunosuppression [25], inflammation (downregulation of *il6*, *crp*, or upregulation of *tgfb*) and/or T cell and macrophage activation [47], may also be performed. Combining the information generated by *in silico* screening with future *in vitro* and *in vivo* experimentation, forms an integrative approach for unrevealling the bio-interactions and effects induced by nGs/nGOs and expanding our knowledge of these highly bio-interactive planar hydrophobic substances.

SUPPORTING INFORMATION

Table S1. Trout CYPs CLUSTAL O(1.2.4) sequence alignment

```
--------------------------------------------------------------------------------
O93299|CP2K3_ONCMY -----MSLIEGLLQTSSTVTL----LGTVLFLLVLY------------LRSSGSSSEGQ 38
Q92110|CP1A1_ONCMY MVLMILPIIGSVSVSEGLVAIVTLCLVYM---LMKY------------KHTEIPEGLKR 44
Q07217|CP11A_ONCMY ---------------MMVSWSVCRSSLALPACGLPSARHNSSMPVVRQALSPDNSSTVQN 45
Q92109|CP1A3_ONCMY MVLMILPIIGSVSASEGLVAMVTLCLVYM---IMKY------------MHTEIPEGLKR 44
Q92090|CP2K1_ONCMY -----MSLIEDILQTSSTVTL----LGTVLFLLVLY------------LRSSGSSSEEQ 38
P30437|CP17A_ONCMY -----------------MAWFLCMCVFSVVGLGLLL------------LQVKLRRSLET 30
Q92088|CP2M1_ONCMY -----MDVL-HILQTNFVSII----IGFVVIILL-W---------------MNRGKQSN 33
O93297|CP2K4_ONCMY -----MSLIEGLLQTSSTVTL----LGTVLFLLVPY------------LRSSGSSSEEQ 38
O42563|CP3AR_ONCMY ----MMSFLPYFS---AETWTLLALLITL---I--V------------VYGYWPYGVFT 35
                                               :
O93299|CP2K3_ONCMY GKEPPGPR--PLPLLGNMLQLD-LKKPYCTLCELSKKYGSIFTFHFGPKKVVVLAGYKTV 95
Q92110|CP1A1_ONCMY LPGPK-----PLPIIGNVLEV--YNNPHLSLTAMSERYGSVFQIQIGMRPVVVLSGNETV 97
Q07217|CP11A_ONCMY FSEIPGLWRNGLANLYSFWKLDGFRNIHRVMVHNFNTFGPIYREKIGYYDSVNIIKPEMP 105
Q92109|CP1A3_ONCMY LPGPK-----PLPIIGNMLEV--HNNPHLSLTAMSERYGSVFQIQIGMRPVVVLSGNETV 97
Q92090|CP2K1_ONCMY GKEPPGPR--PLPLLGNMLQLD-LKKPYCTLCELSKKYGSIFTVHFGPKKVVVLAGYKTV 95
P30437|CP17A_ONCMY RGGPPSLP--VFPLIGSLLSLRSNQAPHVLFQKLQQKYGHTYSLMMGPHTVILVNHHQHA 88
Q92088|CP2M1_ONCMY SRLPPGPA--PIPLLGNLLRMD-VKAPYKLYMELSKKYGSVFTVWLGSKPVVVISGYQAI 90
O93297|CP2K4_ONCMY GKEPPGPR--PLPLLGNMLQLD-LKKPYCTLCELSKKYGSIFTVHFGSKKVVVLAGYKTV 95
O42563|CP3AR_ONCMY KMGIPGPK--PLPYFGTMLEYK--KGFTNFDTECFQKYGRIWGIYDGRQPVLCIMDKSMI 91
                              :  : ..      .          : :*  :    *    : :   .
O93299|CP2K3_ONCMY KQALVNQAED-FGDRDI---TPVFYDF-NQGHGILFA--NGDSWKEMRRFALTNL----- 143
Q92110|CP1A1_ONCMY RQALIKQGED-FAGRPD---LYSFKFI-NDGKSLAFSTDKAGVWRARRKLAMSAL----- 147
Q07217|CP11A_ONCMY AILFKA--EGHYPKRLTVEAWTSYRDYRNRKYGVLLK--NGEDWRSNRVILNREVISPKV 161
Q92109|CP1A3_ONCMY RQALIKQGED-FAGRSD---LYSFKFI-NDGKSLAFSTDKAGVWRARRKLAMSAL----- 147
Q92090|CP2K1_ONCMY KQALVNQAED-FGDRDI---TPVFYDF-NQGHGILFA--NGDSWKEMRRFALTNL----- 143
P30437|CP17A_ONCMY KEVLLKKGKI-FAGRPR---TVTTDLLTRDGKDIAFA-DYGATWRFHRKTVHGAL----- 138
Q92088|CP2M1_ONCMY KDAFVTQGEE-FSGRAN---YPVIMTV-SKGYGVLVS--SGKRSKDLRRFSLMTL----- 138
O93297|CP2K4_ONCMY KQALVNQAED-FGERDI---TPAFYDF-NQGHGILFT--NGDSWKEMRRFALTNL----- 143
O42563|CP3AR_ONCMY KTVLIKECYNIFTNRRN---FHLNGEL-----FDALSVAEDDTWRRIRSVLSPSFTSGRL 143
                      :       :  *                    .        :  *      .
O93299|CP2K3_ONCMY -RDFGMG-KK-------GSEEKILEEIPYLIEVFEKH--EGKAFDTTQSVLYAVSNIISA 192
Q92110|CP1A1_ONCMY -RSFATL-EGTTPEYSCALEEHVCKEGEYLVKQLTSVMDVSGSFDPFRHIVVSVANVICG 205
Q07217|CP11A_ONCMY LGNFVPLLDEVGQDFVARVHKKIER-----------SGQDKWTTDLSQELFKYALESVGS 210
Q92109|CP1A3_ONCMY -RSFATL-EGTTPEYSCALEEHVLKEGEYLVKQLTSVMDVSGSFDPFRHIVVSVANVICG 205
Q92090|CP2K1_ONCMY -RDFGMG-KK-------GSEEKILEEIPYLIEVFEKH--EGKAFDTTQSVLYAVSNIISA 192
P30437|CP17A_ONCMY -CMFGEG-SA-------SIEKIICREALSLCDTLRES--GSASLDLSPELTRAVTNVVCS 187
Q92088|CP2M1_ONCMY -KTFGMG-RR-------SIEERVQEEAKMLVKAFGEY--RDSVVNPKELLCNCVGNVICS 187
O93297|CP2K4_ONCMY -RDFGMG-KK-------GSEEKILEEIPYLIEVLEKH--EGKAFDTTQSVHHAVSNIISA 192
O42563|CP3AR_ONCMY KEMFGIM-KQHSSTLLSGMKKQADKD--------------QTIEVKEFFGPYSMDVVTS 187
                      *               .:   .                   :    .     : : .
O93299|CP2K3_ONCMY IVYGSRF----EYTDPLFTGMADRAKESIHLTGSASIQMYNMFPWLGPWINN-LTRLKK- 246
Q92110|CP1A1_ONCMY MCFGRRY----SHDDQELLGLVNMSDEFGQVVGSG--NPADFIPILRYLPNRTMKRFMD- 258
Q07217|CP11A_ONCMY VLYGERLGLMLDYINPEAQHFIDCISLMFKTTSPMLYIPPAMLRRVGAKIWRDHVEAWDG 270
Q92109|CP1A3_ONCMY MCFGRRY----SHDDQELLGLVNMSDEFGQVVGSG--NPADFIPILRYLPNRTMKRFMD- 258
Q92090|CP2K1_ONCMY IVYGSRF----EYTDPLFTGMADRAKESIHLTGSASIQMYNMFPWLGPWINN-LTRLKK- 246
P30437|CP17A_ONCMY LCFSSSY----CRGDPEFEAMLQFSQGIVDTVAKD--SLVDIFPWLQVFPNADLRLLKQ- 240
Q92088|CP2M1_ONCMY IVFGHRF----ENDDPMFQLIQKAVDAYFNVLSSPIGAMYNMFPRIVWCFPGNHHEMFA- 242
O93297|CP2K4_ONCMY IVYGSRF----EYTDPLFTGMVDRVNENVHLIGSASIQMYNMFPWLGPWINN-LTRLKK- 246
O42563|CP3AR_ONCMY TAFSVDIDSLNNPSDPFVSNVKKMLK---FDLFNPLFLLVALFPFTGPILEKMKFSFFPT 244
                     :.          :     . .  .               ::
O93299|CP2K3_ONCMY NIADMKMEVTELVRGLKETLNPHMCR-GFVDSFLVRKQTLEESGHM-----DSFYHDDNL 300
Q92110|CP1A1_ONCMY INDRFNNFVQKIVSEHYESYDKDNIR-DITDSLIDHCEDRKLDENA-----NIQVSDEKI 312
Q07217|CP11A_ONCMY IFNQADRCIQNIYRTMRQDTNTHGKYPGVLASLLM---------------LDKLSIEDI 314
Q92109|CP1A3_ONCMY INDRFNNFVQKIVSEHYESYDKDNIR-DITDSLIDHCEDRKLDENA-----NIQVSDEKI 312
Q92090|CP2K1_ONCMY NIADMKMEVIELVRGLKETLNPHMCR-GFVDSFLVRKQTLEESGHM-----DSFYHDDNL 300
P30437|CP17A_ONCMY CVSIRDKLLQKKYEEHKSDYSDHEQR-DLLDALLRAKRSAENNNTAEITMETVGLSEDHL 299
Q92088|CP2M1_ONCMY IVNKAKVYIQEQAEIRLKTLNISEPQ-DFIEAFLVKM--LEEKDDP-----NTEFNNGNM 294
O93297|CP2K4_ONCMY NVADLKMEVIELVRGLKETLNPHMCR-GFVDSFLVRKQTLEESGKM-----DSFYHDDNL 300
O42563|CP3AR_ONCMY AVTDFFYASLAKIKSGRDTGNSTNRV-DFLQLMIDSQKGSD---TKTGEEQTKGLTDHEI 300
                                    .  .      ..   ::                        .:

O93299|CP2K3_ONCMY VFSVGNLFSAGTDTTGTTLRWGLLLMTKYPHIQDQVQEEISGVIG-SRQTLVEDRKNLPY 359
Q92110|CP1A1_ONCMY VGIVNDLFGAGFDTISTALSWAVVYLVAYPEIQERLHQELKEKVGMIRTPRLSDKINLPL 372
Q07217|CP11A_ONCMY KASVTELMAGGVDTTSITLLWTLYELARHPDLQEELRAEVAVARQSTQGDMLQMLKMIPL 374
Q92109|CP1A3_ONCMY VGIVNDLFGAGFDTISTALSWAVVYLVAYPETQERLHQELKEKVGMIRTPRLSDKINLPL 372
Q92090|CP2K1_ONCMY VFSVGNLFSAGTDTTGTTLRWGLLLMTKYPHIQDQVQEEISRVIG-SRQTLVEDRKNLPY 359
P30437|CP17A_ONCMY LMTVGDIFGAGVETTSTVLKWAIAYLIHHPQVQQRIQEELDSVVGGDRTPQLSDRGSLPY 359
Q92088|CP2M1_ONCMY VMTAWSLFAAGTETTSSTLRQSFLMMIKYPHIQESVQKEIDEVIG-SRVPTVDDRVKMPY 353
O93297|CP2K4_ONCMY LFSIGNLFGAGTDTTGTTLRWGLLLMAKYPHIQDQVQEEISRVIG-SRQTLVEDRKNLPY 359
O42563|CP3AR_ONCMY LSQAMIFIFAGYETSSSTMSFLAYNLATNHHVMTKLQEEIDTVFPNKAPIQYEALMQMDY 360
                         :: .* :* . .:      :    .    :: *:            .    :
O93299|CP2K3_ONCMY TDAVIHETQRLANIAPMSIPHTTSRDVTFQGYFIKK------------DDSEWESPHTL 406
Q92110|CP1A1_ONCMY LEAFILEIFRHSSFLPFTIPHCTIKDTSLNGYFIPKDTCVFINQWQVNHDPELWKEPSSF 432
Q07217|CP11A_ONCMY VKGALKETLRLHPVAVSL-QRYITEEIVIQNYHIPCGTLVQLGLYAMGRDPDVFPRPEKY 433
Q92109|CP1A3_ONCMY LEAFILEIFRHSSFLPFTIPHCTIKDTSLNGYFIPKDTCVFINQWQVNHDPELWKEPSSF 432
Q92090|CP2K1_ONCMY TDAVIHETQRLANIVPMSVPHTTSRDVTFQGYFIKKGTSVIPLLTSVLQDDSEWESPNTF 419
P30437|CP17A_ONCMY LEATIREVLRIRPVAPLLIPHVAQTDTSIGKFTVRKGARIIINLWSLHHDEKEWKNPEMF 419
Q92088|CP2M1_ONCMY TDAVIHEVQRYMDLSPTSVPHKVMRDTEFYNYHIPEGTMVLPLLSSVLVDPKLFKNPDEF 413
O93297|CP2K4_ONCMY TDAVIHETQRLANISPMAVPHTTSRDVTFQGYFIKKGTSVIPLLMSVLQDDNEWESPNTF 419
O42563|CP3AR_ONCMY LDCVLNESLRLYPIAPRL-ERVAKKTVEINGIVIPKDCIVLVPTWTLHRDPEIWSDPEEF 419
                    .  : *  *   .      :       :    :               * . :  *
O93299|CP2K3_ONCMY TPSHFLDEKGGFV---KRDAFMAFSAGRRVCLGEGLARMELFLFFTSLLQHFRFSPPPGV 463
Q92110|CP1A1_ONCMY NPDRFLSADGTELNKLEGEKVLVFGMDKRRCIGEAIGRNEVYLFLAILLQRLRFQEKPGH 492
Q07217|CP11A_ONCMY LPSRWLRTENQYF------RSLGFGFGPRQCLGRRIAETEMQLFLIHMLENFRVDKQRQV 487
Q92109|CP1A3_ONCMY NPDRFLSADGTELNKLEGEKVLVFGMGKRRCIGEAIGRNEVYLFLAILLQRLRFQEKPGH 492
Q92090|CP2K1_ONCMY NPSHFLDEQGGFV---KRDAFMAFSAGRRVCLGEGLARMELFLFFTSLLQRFRFSPPPGV 476
P30437|CP17A_ONCMY DPGRFLNEEGTGLCI-PSPSYLPFGAGVRVCLGEALAKMEIFLFLSWILQRLTMTVSPGQ 478
Q92088|CP2M1_ONCMY DPENFLDENGVFK---KNDGFFAFGVGKRACPGEALARVELFLFFTSVLQRFTFTGTKPP 470
O93297|CP2K4_ONCMY NPSHFLDEQGGFV---KRDAFMAFSAGRRVCLGEGLARMELFLFFTSLLQRFRFSPPPGV 476
O42563|CP3AR_ONCMY KPERFSKENKESI---DPYTYMPFGAGPRNCIGMRFALIMIKLAMVEILQSFTFSVCDET 476
                    * .:   .            : *. . * C *  :.   : * :  :*: : .
O93299|CP2K3_ONCMY TEDDLDLTPSVE-FTHNPSP--HQLCAVSRV---------------- 491
Q92110|CP1A1_ONCMY PLDMT------PEYGLTMKH---KRCQLKASM-RPWGQEE-------- 522
Q07217|CP11A_ONCMY EVHST--------FELILLPEKPILLTLKPLKS---GQ---------- 514
Q92109|CP1A3_ONCMY PLDMT------PEYGLTMKH---KRCQLKASM-RPWGQEE-------- 522
Q92090|CP2K1_ONCMY TEDDLDLTPLLG-FTLNPSP--HQLCAVSRV---------------- 504
P30437|CP17A_ONCMY PLPSL--E---GKFGVVLQP---VKYKVNATPRAGWEKSH--LQTS-- 514
Q92088|CP2M1_ONCMY EEI--NIEPACSSFGRLPRS---YDCYIKLRTEK------------- 499
O93297|CP2K4_ONCMY TEDDLDLTPLLG-FTLHPSP--HQLCAVSRV---------------- 504
O42563|CP3AR_ONCMY EIPLE-----MDNQGLLMPK-RPIKLRLEARRNTPSNTTATTLKSPTT 518
                                         :.
--------------------------------------------------------------------------------
```

Conserved Cysteins are in bold and green backgrounds while other conserved amino acids in all trout CYPs and/or their similar surrounding amino acids to such positions are in bold red lettering. Similar conserved amino acids (:.).

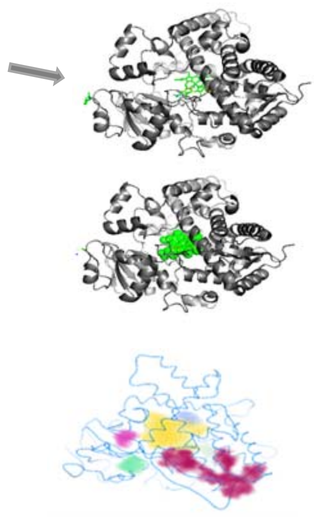

Figure S1. 2D scheme of trout modelled CYP molecule and its predicted binding pockets. The figure shows the amino acid sequence in grey and the heme in green (up in lines and down in spheres) occupying an internal part of CYPs. A tunnel-like with an opening to the left in the drawing (Grey arrow) may support a possible way through which substrates and/or inhibitors may get close to the heme for optimal oxidation (ligand binding pocket). Most of the crystalized ligands map to that heme binding-pocket (yellow background). Between 6-15 other binding pockets were predicted by seeSAR depending on the CYPs (different color backgrounds in the down figure)

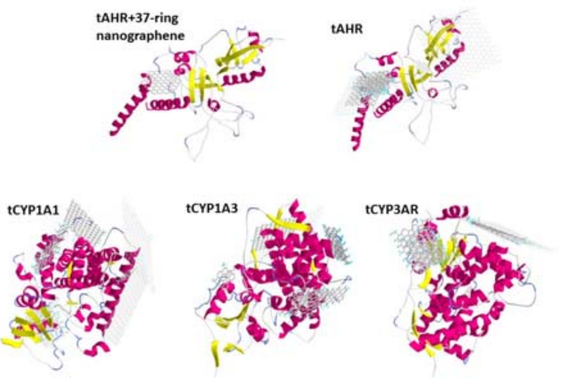

Figure S2. Drawings of nGs of different sizes bound to tAHR (up) and tCYPS (down). AutoDock Vina used a whole molecule grid (blind-docking). The nGs of 4 (5x5 nm), 9 (7x7 nm), 12 (10x10 nm), 20 (12x12 nm), 25 (13x13 nm), 36 (15x15 nm), 72 (20x20 nm), 100 (25x25 nm), and 156 (30x30 nm) rings were designed using the GOPY tool. Representative cartoons were made by combining one molecule of protein with several sizes of nG molecules and drawn in PyRx. The heme at the inner part of the CYP molecules have been removed for clarity.

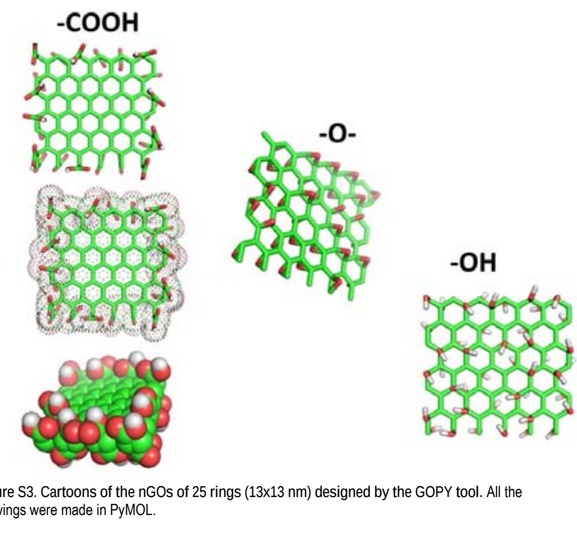

Figure S3. Cartoons of the nGOs of 25 rings (13x13 nm) designed by the GOPY tool. All the drawings were made in PyMOL.

Funding
This research was funded in part by the European Union's Horizon 2020 research and innovation programme (NanoReg2, Grant Agreement nº 646221).

Competing interests
The authors declare that they have no competing interests

Authors' contributions
MC and JN, collaborated by critically discussing strategies and writing and correcting the manuscript. JC performed and analyzed the computational work and drafted the manuscript. Authors read and approved the manuscript.

Acknowledgements
Thanks are due to Dra Ana Valdehita for her help to obtain additional seeSAR licenses. Mona Connolly received financing granted by the Community of Madrid (2018-T2/AMB-11392, Mode 2, Young Doctor Recruiment).

References

[1] Dasari Shareena, T.P., D. McShan, A.K. Dasmahapatra and P.B. Tchounwou.A Review on Graphene-Based Nanomaterials in Biomedical Applications and Risks in Environment and Health *Nanomicro Lett.* 2018, 10.https://dx.doi.org/10.1007/s40820-018-0206-4

[2] Ema, M., M. Gamo and K. Honda.A review of toxicity studies on graphene-based nanomaterials in laboratory animals *Regul Toxicol Pharmacol.* 2017, 85: 7-24.https://dx.doi.org/10.1016/j.yrtph.2017.01.011

[3] Xiong, G., Y. Deng, X. Liao, J. Zhang, B. Cheng, Z. Cao and H. Lu.Graphene oxide nanoparticles induce hepatic dysfunction through the regulation of innate immune signaling in zebrafish (Danio rerio) *Nanotoxicology.* 2020: 1-16.https://dx.doi.org/10.1080/17435390.2020.1735552

[4] Ou, L., B. Song, H. Liang, J. Liu, X. Feng, B. Deng, . . . L. Shao.Toxicity of graphene-family nanoparticles: a general review of the origins and mechanisms *Part Fibre Toxicol.* 2016, 13: 57.https://dx.doi.org/10.1186/s12989-016-0168-y 10.1186/s12989-016-0168-y [pii]

[5] Lammel, T., P. Boisseaux and J.M. Navas.Potentiating effect of graphene nanomaterials on aromatic environmental pollutant-induced cytochrome P450 1A expression in the topminnow fish hepatoma cell line PLHC-1 *Environ Toxicol.* 2015, 30: 1192-204.https://dx.doi.org/10.1002/tox.21991

[6] Pan, Y., C.E. Ong, Y.F. Pung and J.Y. Chieng.The current understanding of the interactions between nanoparticles and cytochrome P450 enzymes - a literature-based review *Xenobiotica.* 2019, 49: 863-876.https://dx.doi.org/10.1080/00498254.2018.1503360

[7] Orecchioni, M., D. Bedognetti, F. Sgarrella, F.M. Marincola, A. Bianco and L.G. Delogu.Impact of carbon nanotubes and graphene on immune cells *J Transl Med.* 2014, 12: 138.1479-5876-12-138 [pii] https://dx.doi.org/10.1186/1479-5876-12-138

[8] Orecchioni, M., D.A. Jasim, M. Pescatori, R. Manetti, C. Fozza, F. Sgarrella, . . . L.G. Delogu.Molecular and Genomic Impact of Large and Small Lateral Dimension Graphene Oxide Sheets on Human Immune Cells from Healthy Donors *Adv Healthc Mater.* 2016, 5: 276-87.https://dx.doi.org/10.1002/adhm.201500606

[9] Orecchioni, M., C. Menard-Moyon, L.G. Delogu and A. Bianco.Graphene and the immune system: Challenges and potentiality *Adv Drug Deliv Rev.* 2016, 105: 163-175.S0169-409X(16)30156-9 [pii] https://dx.doi.org/10.1016/j.addr.2016.05.014

[10] Lammel, T., P. Boisseaux, M.L. Fernandez-Cruz and J.M. Navas.Internalization and cytotoxicity of graphene oxide and carboxyl graphene nanoplatelets in the human hepatocellular carcinoma cell line Hep G2 *Part Fibre Toxicol.* 2013, 10: 27.1743-8977-10-27 [pii] https://dx.doi.org/10.1186/1743-8977-10-27

[11] Markovic, M., A. Kumar, I. Andjelkovic, S. Lath, J.K. Kirby, D. Losic, . . . M.J. McLaughlin.Ecotoxicology of manufactured graphene oxide nanomaterials and derivation of preliminary guideline values for freshwater environments *Environ Toxicol Chem.* 2018, 37: 1340-1348.https://dx.doi.org/10.1002/etc.4074

[12] Markovic, M., I. Andelkovic, J. Shuster, L. Janik, A. Kumar, D. Losic and M.J. McLaughlin.Addressing challenges in providing a reliable ecotoxicology data for graphene-oxide (GO) using an algae (Raphidocelis subcapitata), and the trophic transfer consequence of GO-algae aggregates *Chemosphere.* 2020, 245: 125640.S0045-6535(19)32880-2 [pii] https://dx.doi.org/10.1016/j.chemosphere.2019.125640

[13] Kurapati, R., C. Backes, C. Menard-Moyon, J.N. Coleman and A. Bianco.White Graphene undergoes Peroxidase Degradation *Angew Chem Int Ed Engl.* 2016, 55: 5506-11.https://dx.doi.org/10.1002/anie.201601238

[14] Kurapati, R. and A. Bianco.Peroxidase mimicking DNAzymes degrade graphene oxide *Nanoscale.* 2018, 10: 19316-19321.https://dx.doi.org/10.1039/c8nr06535q

[15] Grans, J., B. Wassmur and M.C. Celander.One-way inhibiting cross-talk between arylhydrocarbon receptor (AhR) and estrogen receptor (ER) signaling in primary cultures of rainbow trout hepatocytes *Aquat Toxicol.* 2010, 100: 263-70.S0166-445X(10)00272-9 [pii] https://dx.doi.org/10.1016/j.aquatox.2010.07.024

[16] Grans, J., B. Wassmur, M. Fernandez-Santoscoy, J. Zanette, B.R. Woodin, S.I. Karchner, . . . M.C. Celander.Regulation of pregnane-X-receptor, CYP3A and P-glycoprotein genes in the PCB-resistant killifish (Fundulus heteroclitus) population from New Bedford Harbor *Aquat Toxicol.* 2015, 159: 198-207.S0166-445X(14)00383-X [pii] https://dx.doi.org/10.1016/j.aquatox.2014.12.010

[17] Fukunaga, B.N., M.R. Probst, S. Reisz-Porszasz and O. Hankinson.Identification of functional domains of the aryl hydrocarbon receptor *J Biol Chem.* 1995, 270: 29270-8.https://dx.doi.org/10.1074/jbc.270.49.29270

[18] Whitlock, J.P., Jr.Induction of cytochrome P4501A1 *Annu Rev Pharmacol Toxicol.* 1999, 39: 103-25.https://dx.doi.org/10.1146/annurev.pharmtox.39.1.103

[19] Poland, A., D. Palen and E. Glover.Analysis of the four alleles of the murine aryl hydrocarbon receptor *Mol Pharmacol.* 1994, 46: 915-21.not doi

[20] Wassmur, B., J. Grans, P. Kling and M.C. Celander.Interactions of pharmaceuticals and other xenobiotics on hepatic pregnane X receptor and cytochrome P450 3A signaling pathway in rainbow trout (Oncorhynchus mykiss) *Aquat Toxicol.* 2010, 100: 91-100.S0166-445X(10)00261-4 [pii] https://dx.doi.org/10.1016/j.aquatox.2010.07.013

[21] Renaud, H.J., J.Y. Cui, M. Khan and C.D. Klaassen.Tissue distribution and gender-divergent expression of 78 cytochrome P450 mRNAs in mice *Toxicol Sci.* 2011, 124: 261-77.kfr240 [pii], http://dx.doi.org/10.1093/toxsci/kfr240

[22] Uno, T., M. Ishizuka and T. Itakura.Cytochrome P450 (CYP) in fish *Environ Toxicol Pharmacol.* 2012, 34: 1-13.S1382-6689(12)00016-6 [pii] https://dx.doi.org/10.1016/j.etap.2012.02.004

[23] Jonsson, M.E., K. Gao, J.A. Olsson, J.V. Goldstone and I. Brandt.Induction patterns of new CYP1 genes in environmentally exposed rainbow trout *Aquat Toxicol.* 2010, 98: 311-21.S0166-445X(10)00088-3 [pii] https://dx.doi.org/10.1016/j.aquatox.2010.03.003

[24] Katagi, T.In vitro metabolism of pesticides and industrial chemicals in fish *J Pestic Sci.* 2020, 45: 1-15.https://dx.doi.org/10.1584/jpestics.D19-074

[25] Effner, R., J. Hiller, S. Eyerich, C. Traidl-Hoffmann, K. Brockow, M. Triggiani, . . . J.T. Buters.Cytochrome P450s in human immune cells regulate IL-22 and c-Kit via an AHR feedback loop *Sci Rep.* 2017, 7: 44005.srep44005 [pii] http://dx.doi.org/10.1038/srep44005

[26] Stavropoulou, E., G.G. Pircalabioru and E. Bezirtzoglou.The Role of Cytochromes P450 in Infection *Front Immunol.* 2018, 9: 89.https://dx.doi.org/10.3389/fimmu.2018.00089

[27] Muntane-Relat, J., J.C. Ourlin, J. Domergue and P. Maurel.Differential effects of cytokines on the inducible expression of CYP1A1, CYP1A2, and CYP3A4 in human hepatocytes in primary culture *Hepatology.* 1995, 22: 1143-53.https://dx.doi.org/S0270913995003569 [pii]

[28] Bello-Perez, M., A. Falco, B. Novoa, L. Perez and J. Coll.Hydroxycholesterol binds and enhances the anti-viral activities of zebrafish monomeric c-reactive protein isoforms *PLoS One.* 2019, 14: e0201509.http://dx.doi.org/10.1371/journal.pone.0201509

[29] Tian, S., Y. Djoumbou-Feunang, R. Greiner and D.S. Wishart.CypReact: A Software Tool for in Silico Reactant Prediction for Human Cytochrome P450 Enzymes *J Chem Inf Model.* 2018, 58: 1282-1291.http://dx.doi.org/10.1021/acs.jcim.8b00035

[30] Tan, B.H., Y. Pan, A.N. Dong and C.E. Ong.In vitro and in silico Approaches to Study Cytochrome P450-Mediated Interactions *J Pharm Pharm Sci.* 2017, 20: 319-328.http://dx.doi.org/10.18433/J3434R

[31] Zhang, T., Q. Chen, L. Li, L.A. Liu and D.Q. Wei.In silico prediction of cytochrome P450-mediated drug metabolism *Comb Chem High Throughput Screen.* 2011, 14: 388-95.BSP/CCHTS/E-Pub/00153 [pii] https://dx.doi.org/10.2174/138620711795508412

[32] Lammel, T. and J.M. Navas.Graphene nanoplatelets spontaneously translocate into the cytosol and physically interact with cellular organelles in the fish cell line PLHC-1 *Aquat Toxicol.* 2014, 150: 55-65.S0166-445X(14)00066-6 [pii] https://dx.doi.org/10.1016/j.aquatox.2014.02.016

[33] Muraru, S., J.S. Burns and M. Ionita.GOPY: a tool for building 2D graphene-based computational models *SoftwareX.* 2020, 12: 100586.https://doi.org/10.1016/j.softx.2020.100586

[34] Andon, F.T., A.A. Kapralov, N. Yanamala, W. Feng, A. Baygan, B.J. Chambers, . . . V.E. Kagan.Biodegradation of single-walled carbon nanotubes by eosinophil peroxidase *Small.* 2013, 9: 2721-9, 2720.https://dx.doi.org/10.1002/smll.201202508

[35] Trott, O. and A.J. Olson.AutoDock Vina: improving the speed and accuracy of docking with a new scoring function, efficient optimization, and multithreading *J Comput Chem.* 2010, 31: 455-61.http://dx.doi.org/10.1002/jcc.21334

[36] Dallakyan, S. and A.J. Olson.Small-molecule library screening by docking with PyRx *Methods Mol Biol.* 2015, 1263: 243-50.http://dx.doi.org/10.1007/978-1-4939-2269-7_19

[37] Blasco, R. and J.M. Coll.In silico screening for natural ligands to non-structural nsp7 conformers of SARS coronaviruses *ChemRxiv.* 2020.https://doi.org/10.26434/chemrxiv.12952115.v2

[38] Coll, J.M.Would it be possible to stabilize prefusion SARS-COV-2 spikes with ligands? *ChemRxiv.* 2020.https://doi.org/10.26434/chemrxiv.13453919.v1

[39] Shityakov, S. and C. Forster.In silico predictive model to determine vector-mediated transport properties for the blood-brain barrier choline transporter *Adv Appl Bioinform Chem.* 2014, 7: 23-36.http://dx.doi.org/10.2147/AABC.S63749

[40] Reau, M., F. Langenfeld, J.F. Zagury and M. Montes.Predicting the affinity of Farnesoid X Receptor ligands through a hierarchical ranking protocol: a D3R Grand Challenge 2 case study *J Comput Aided Mol Des.* 2018, 32: 231-238.10.1007/s10822-017-0063-0 [pii] http://dx.doi.org/10.1007/s10822-017-0063-0

[41] Schneider, N., S. Hindle, G. Lange, R. Klein, J. Albrecht, H. Briem, . . . M. Rarey.Substantial improvements in large-scale redocking and screening using the novel HYDE scoring function *J Comput Aided Mol Des.* 2012, 26: 701-23. http://dx.doi.org/10.1007/s10822-011-9531-0

[42] Schneider, N., G. Lange, S. Hindle, R. Klein and M. Rarey.A consistent description of HYdrogen bond and DEhydration energies in protein-ligand complexes: methods behind the HYDE scoring function *J Comput Aided Mol Des.* 2013, 27: 15-29. http://dx.doi.org/10.1007/s10822-012-9626-2

[43] Martignoni, M., G.M. Groothuis and R. de Kanter.Species differences between mouse, rat, dog, monkey and human CYP-mediated drug metabolism, inhibition and induction *Expert Opin Drug Metab Toxicol.* 2006, 2: 875-94.https://dx.doi.org/10.1517/17425255.2.6.875

[44] Celander, M., D.R. Buhler, L. Forlin, A. Goksoyr, C.L. Miranda, B.R. Woodin and J.J. Stegeman.Immunochemical relationships of cytochrome P4503A-like proteins in teleost fish *Fish Physiol Biochem.* 1996, 15: 323-32.10.1007/BF02112359

[45] Connors, K.A., B. Du, P.N. Fitzsimmons, A.D. Hoffman, C.K. Chambliss, J.W. Nichols and B.W. Brooks.Comparative pharmaceutical metabolism by rainbow trout (Oncorhynchus mykiss) liver S9 fractions *Environ Toxicol Chem.* 2013, 32: 1810-8.http://dx.doi.org/10.1002/etc.2240

[46] Ambrosio, L.F., C. Insfran, X. Volpini, E. Acosta Rodriguez, H.M. Serra, F.J. Quintana, . . . C.C. Motran.Role of Aryl Hydrocarbon Receptor (AhR) in the Regulation of Immunity and Immunopathology During Trypanosoma cruzi Infection *Front Immunol.* 2019, 10: 631.http://dx.doi.org/10.3389/fimmu.2019.00631

[47] Abdullah, A., M. Maged, M.I. Hairul-Islam, I.A. Osama, H. Maha, A. Manal and H. Hamza.Activation of aryl hydrocarbon receptor signaling by a novel agonist ameliorates autoimmune encephalomyelitis *PLoS One.* 2019, 14: e0215981.http://dx.doi.org/10.1371/journal.pone.0215981 PONE-D-18-33358 [pii]